Bioorganic Chemistry 110 (2021) 104805

Contents lists available at ScienceDirect

Bioorganic Chemistry

journal homepage: www.elsevier.com/locate/bioorg

# Synthesis and anticancer evaluation of 6-azacyclonol-2,4,6-trimethylpyridin-3-ol derivatives: M3 muscarinic acetylcholine receptor-mediated anticancer activity of a cyclohexyl derivative in androgen-refractory prostate cancer

Ujjwala Karmacharya [a,1], Prakash Chaudhary [a,1], Dongchul Lim [b], Sadan Dahal [a], Bhuwan Prasad Awasthi [a], Hee Dong Park [b], Jung-Ae Kim [a,*], Byeong-Seon Jeong [a,*]

[a] College of Pharmacy, Yeungnam University, 280 Daehak-ro, Gyeongsan 38541, Republic of Korea
[b] Innovo Therapeutics Inc., Daeduck Biz Center C-313, 17 Techno 4-ro, Yuseong-gu, Daejeon 34013, Republic of Korea

ARTICLE INFO

*Keywords:*
Chemical modification
Androgen-refractory prostate cancer (ARPC)
Antitumor
DeepZema
M3 muscarinic acetylcholine receptor (M3R)

ABSTRACT

We recently reported 2,4,5-trimethylpyridin-3-ol with C(6)-azacyclonol, whose code name is BJ-1207, showing a promising anticancer activity by inhibiting NOX-derived ROS in A549 human lung cancer cells. The present study was focused on structural modification of the azacyclonol moiety of BJ-1207 to find a compound with better anticancer activity. Ten new compounds (**3A**–**3J**) were prepared and evaluated their inhibitory actions against proliferation of eighteen cancer cell lines as a primary screening. Among the ten derivatives of BJ-1207, the effects of compounds **3A** and **3J** on DU145 and PC-3, androgen-refractory cancer cell lines (ARPC), were greater than the parent compound, and compound **3A** showed better activity than **3J**. Antitumor activity of compound **3A** was also observed in DU145-xenografted chorioallantoic membrane (CAM) tumor model. In addition, the ligand-based target prediction and molecular docking study using DeepZema® server showed compound **3A** was a ligand to M3 muscarinic acetylcholine receptor (M3R) which is overexpressed in ARPC. Carbachol, a muscarinic receptor agonist, concentration dependently increased proliferation of DU145 in the absence of serum, and it also activated NADPH oxidase (NOX). The carbachol-induced proliferation and NOX activity was significantly blocked by compounds **3A** in a concentration-dependent manner. This finding might become a new milestone in the development of pyridinol-based anti-cancer agents against ARPC.

## 1. Introduction

Prostate cancer is the most frequently diagnosed cancer and the second leading cause of cancer mortality in men worldwide [1]. At initial diagnosis, prostate cancer is sensitive to chemical or surgical castration therapies that inhibit or deplete androgen action for prostate cancer growth. However, the cancer eventually turns out to be androgen-independent and undergo metastasis, which is referred to as castration-resistant or androgen-refractory prostate cancer (ARPC).

The underlying mechanisms involved in the development of androgen adaptation and therapeutic resistance of ARPC are related to the progression of various mutations in the cancer genome and positive regulatory signals from the tumor microenvironment [2]. Accumulating evidence shows muscarinic receptors, G-protein coupled receptors (GPCRs), and their ligand, acetylcholine, are involved in the growth and progression of prostate cancer [3,4]. Among five subtypes (M1R–M5R) of muscarinic acetylcholine receptors, M1R and M3R are highly upregulated in ARPC compared with hormone-sensitive prostate cancer in cell lines and clinical specimens [3,5]. Also, the abnormal expression of M1R and M3R corresponds to the poor prognosis of progression-free survival in ARPC patients [6]. Because both M1R and M3R receptors share common G protein involvement of coupling to $G_{q/11}$ G proteins, phospholipase C and consequent activation of protein kinase C may be involved in the progression. Several different signaling pathways of M1R and M3R have been reported to induce ARPC progression; hedgehog [4] and FAK-YAP (Focal adhesion kinase-Yes-associated protein) signaling

* Corresponding authors.
*E-mail addresses:* jakim@yu.ac.kr (J.-A. Kim), jeongb@ynu.ac.kr (B.-S. Jeong).
[1] Both authors contributed equally to this work.

https://doi.org/10.1016/j.bioorg.2021.104805
Received 10 January 2021; Received in revised form 20 February 2021; Accepted 2 March 2021
Available online 6 March 2021

[6].

Epidemiological and clinical studies have demonstrated oxidative stress plays a critical role in the development and progression of prostate cancer [7]. ARPC cells produce a higher level of reactive oxygen species (ROS) than androgen-dependent prostate cancer cells. The major ROS source in cancer is NADPH oxidase (NOX), and prostate cancer cells express various NOX isoforms, including NOX1, NOX2, NOX4, and NOX5 [8]. NOX activation is induced by stimuli such as growth factors, cytokines, and calcium influx [9]. Upon stimulation, translocation and unification of cytosolic subunits to membrane components require phosphorylation by various protein kinases, including protein kinase B and protein kinase C [10].

We recently reported a 2,4,5-trimethylpyridin-3-ol compound containing azacyclonol moiety at C(6)-position of the pyridine ring, whose code name is BJ-1207 (**2**) (Fig. 1), showed a promising anticancer activity by inhibiting NOX-derived ROS in A549 human lung cancer cell line [11]. The present study began with a focus on structural modification of BJ-1207 to find a compound showing better anticancer activity by fine-tuning the azacyclonol moiety using its similar substructures. We found that compound **3A**, one of the BJ-1207 derivatives, showed more potent antiproliferative activity than BJ-1207 against human prostate cancer cell lines from this study. In particular, the antiproliferative effect of compound **3A** was better in ARPC cell lines like DU145 and PC-3 than in androgen-sensitive cells such as LNCaP. We also found that the anticancer effect of compound **3A** is mediated through inhibition of M3R, which was revealed by molecular docking analysis, receptor binding assay, and carbachol-induced NOX activation and DU145 cell proliferation assays.

## 2. Results and discussion

### 2.1. Synthesis

In the previous study, BJ-1207 showed the most potent anticancer activity among the fifty compounds **1** used [11]. Since the 2,4,5-trimethylpyridin-3-ol part is common to all fifty compounds, it can be said that the variation in anticancer activity between each compound may be due to the difference in the structure of amino moiety connected to C(6)-position of the pyridine ring. The 6-amino part in BJ-1207 compound is 4-(hydroxydiphenylmethyl)piperidine, also known as azacyclonol, which is the parent structure of fexofenadine, an antihistamine drug used in the treatment of allergy symptoms.

Therefore, this study was mainly focused on exploring the structure–activity relationship on the azacyclonol moiety of BJ-1207, and its ten representative analogs **3A**–**3J** were proposed for this purpose as shown in Fig. 2. Palladium-catalyzed amination was used as an assembly reaction between the key intermediate bromopyridine **4** and ten different cyclic amines **5**.

The synthesis began with the preparation of the common key intermediate (**4**) from commercially available pyridoxine hydrochloride (**6**) following the well-established method developed by us (Scheme 1) [12]. Chlorination of two hydroxyl moieties of **6** was done using excess thionyl chloride and a catalytic amount of *N*,*N*-dimethylformamide. The product thus obtained was refluxed in acetic acid using zinc to cut off the two chlorine groups affording 3-hydroxy-2,4,5-trimethylpyridine (**7**) in a two-step reaction with an overall yield 85% from **6**. Next, bromination and benzylation were done consecutively using 1,3-dibromo-5,5-dimethylhydantoin in the first reaction to introduce bromine for the palladium-catalyzed amination and using benzyl bromide for hydroxyl protection. Commercially available 4-benzoylpiperdine hydrochloride (**8**) was used for the synthesis of the compound **3A**–**3C**. First, the free amino group of **8** was protected from strong basic conditions of the upcoming step by either Cbz or Boc. The addition of the carbonyl of **9-1** with cyclohexylmagnesium bromide gave **10A** in 99% yield [13]. While the commercially available Grignard reagent was used for the synthesis of **10A**, Grignard reagents for **10B** and **10C** were prepared by a halogen-metal exchange reaction using 3-bromothiophene and *n*-butyllithium for **10B** and 2-bromopyridine and isopropylmagnesium chloride for **10C**,

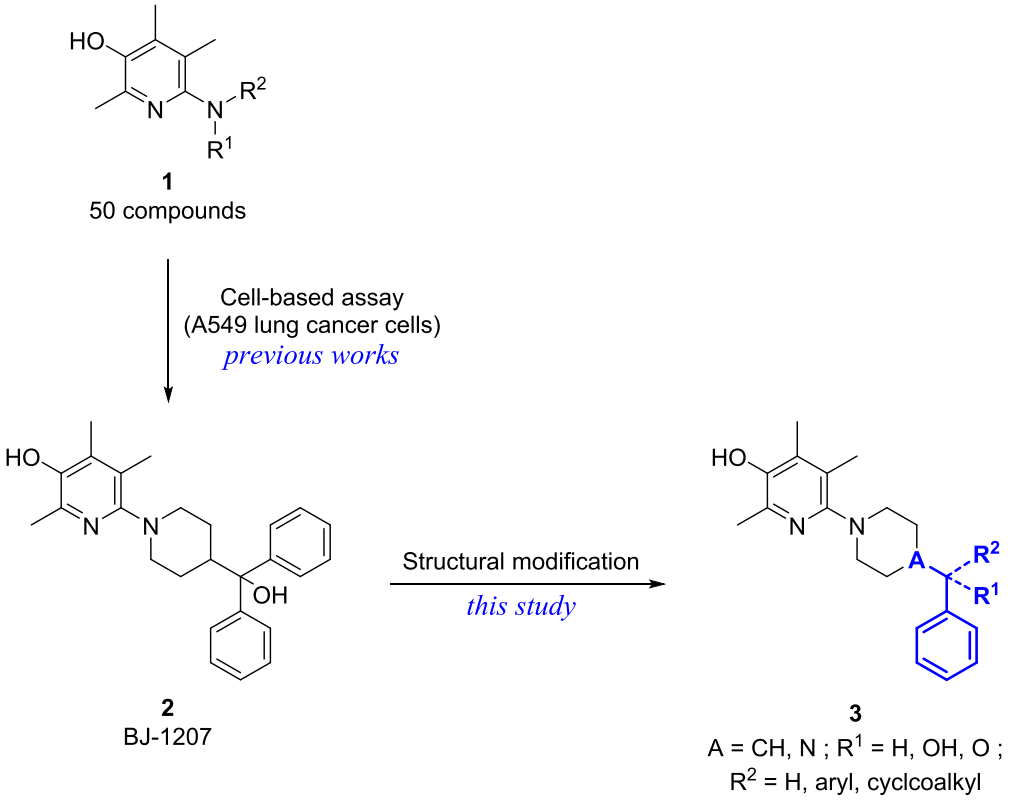


**Fig. 1.** The goal of this study: Structural modification of BJ-1207 by fine-tuning of the azacyclonol moiety.

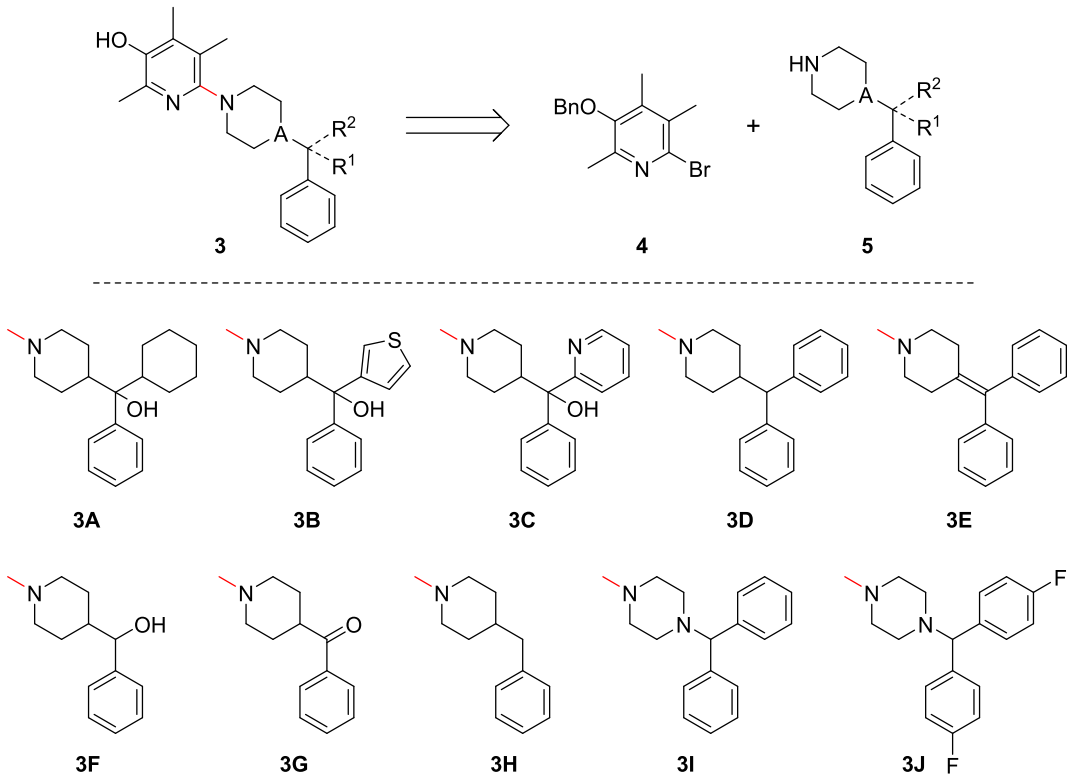


**Fig. 2.** General synthetic strategy for compounds **3** and structures of the derivatives.

respectively. After the Grignard reactions, the protecting group was removed for the next Buchwald-Hartwig amination reaction. For the Cbz protective group in **10A**, deprotection was readily carried out by catalytic hydrogenolysis. However, in the case of **10B**, the reaction did not proceed well under the same reaction conditions, which might be due to deactivation of the palladium catalyst on activated carbon by sulfur atom in the structure of **10B** [13]. Thus, an alternative approach for the removal of Cbz in **10B** was applied. The free piperidine compound **11B** was obtained in a high yield by treatment of **10B** with an excess amount of base in sealed-tube for a long time at high temperature. Typical reaction conditions for the deprotection of Boc group afforded **11C**. All obtained piperidine substrates **11A**–**11C** were then coupled with the bromo-compound **4** under Buchwald-Hartwig amination conditions. Finally, the benzyl protective group was cleaved by catalytic hydrogenolysis using hydrogen gas to get **3A** and **3B**. **3C** was obtained by a milder reaction condition using boron trichloride and pentamethylbenzene. Unlike the case of the deprotection of Cbz of **10B** by catalytic hydrogenolysis, there was no such a problem observed in the transformation of **11B** to **3B**.

Commercially available 4-(hydroxydiphenylmethyl)piperidine (**13**) was employed for the synthesis of two derivatives **3D** and **3E** as shown in Scheme 2. Reductive removal of the hydroxyl group in **13** was done under Gribble reduction conditions, sodium borohydride in trifluoroacetic acid, affording 4-diphenylmethylpiperidine (**14**) in good yield [14,15]. Dehydration reaction of **13** under acidic conditions with trifluoroacetic acid gave 4-(diphenylmethylene)piperidine (**16**) [16]. Both intermediates **14** and **16** were then coupled with the key intermediate **4** by Buchwald-Hartwig amination reaction to get **15** and **17**, respectively. Both were then debenzylated by hydrogenolysis to obtain **3D** and **3E** (see Scheme 3).

On following common sequence of Buchwald-Hartwig reaction of **4** with commercially available reagents, 4-benzoylpiperidine hydrochloride (**8**) and 4-benylpiperidine (**20**), respectively resulted in **18** and **21** while coupling with commercially available 1-benzhydrylpiperazine (**22**) and 1-(bis(4-fluorophenyl)-methyl)piperazine (**24**) gave **23** and **25**, respectively. Then, the final target compounds **3G**–**3J** were obtained by debenzylation either with molecular hydrogen or boron trichloride. On treating the intermediate **18** with sodium borohydride, the corresponding alcohol **19** was formed which was then treated with molecular hydrogen to obtain **3F** [17].

### 2.2. Anticancer activity evaluation

The new compounds **3A**–**3J** along with BJ-1207 (**2**) at one fixed concentration (30 μM) were tested for antiproliferative activity in eighteen different human cancer cell lines: breast cancer cell lines (MCF-7, MCF-7/ADR, MCF-7/TAMR, and MDA-MB-231), colon cancer cell lines (HT-29, SW620, Caco-2, and HCT-116), pancreatic cancer cell lines (PANC-1 and MiaPaCa-2), a liver cancer cell line (Hep3B), lung cancer cell lines (A549 and H1299), prostate cancer cell lines (DU145 and PC-3), monoblastic leukemia cell lines (U937 and THP-1) and a glioblastoma cell line (A172) (Fig. 3). Antiproliferative activities of the new compounds were less effective than the parent compound **2** except compounds **3A** and **3J**. Looking more specifically, replacing one of the phenyl rings of the azacyclonol group in the parent compound **2** with a cyclic alkane (cyclohexyl (**3A**)) or two heteroaromatic rings (thiophen-3-yl (**3B**) and pyridin-2-yl (**3C**)) produced opposite results. The cyclohexyl analogue **3A** showed comparable inhibitory activity in most cancer cell lines to the parent compound **2** at a fixed concentration. In particular, the proliferation of DU145, a prostate cancer cell line, was highly suppressed by compound **3A** (71.3% inhibition) compared to compound **2** (49.0% inhibition). On the other hand, compounds **3B** and **3C**, replaced by heteroaromatic rings, significantly lost the inhibitory activity. Removal of the hydroxyl group of azacyclonol as in analogues **3D** and **3E** was detrimental to the inhibitory activity. Another group of analogues, **3F**, **3G**, and **3I**, in which one of the two phenyl rings of the parent compound was removed, generally showed a decrease in the inhibitory activity regardless of the structural change of the hydroxyl group. Interestingly, the two piperazine analogues with no hydroxyl group, **3I** and **3J**, showed significantly different activity. The inhibitory

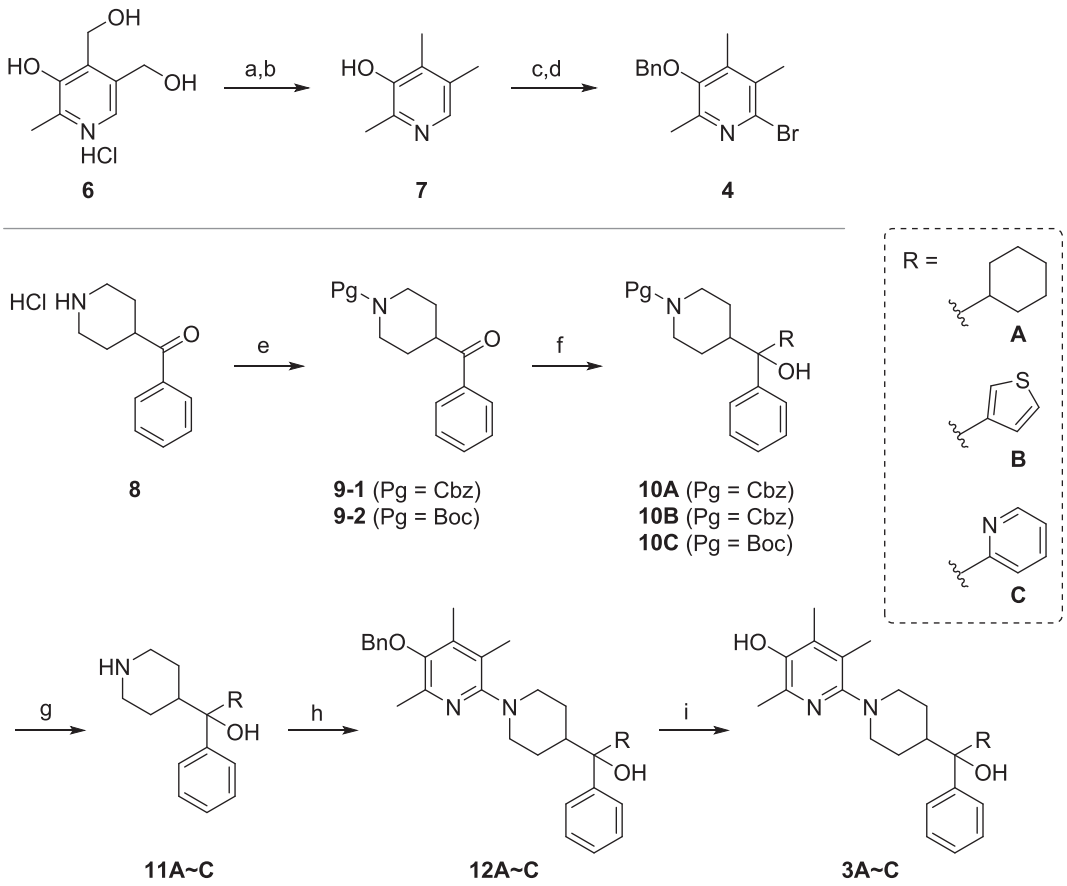


**Scheme 1.** Synthesis of compounds **3A–C**. *Reagents and Conditions*: (a) $SOCl_2$, DMF, reflux, 1 h; (b) Zn, AcOH, reflux, 12 h, 85% (2 steps); (c) DBDMH, THF, r.t., 3 h, 80%; (d) $PhCH_2Br$, $K_2CO_3$, DMF, r.t., 12 h, 87%; (e) for **9-1**: $ClCO_2Bn$, $K_2CO_3$, THF, r.t., 2 h, 90%, for **9-2**: $Boc_2O$, $Et_3N$, DMAP, r.t., 3 h, 66%; (f) for **10A**: *c*-$C_6H_{11}MgBr$, $Et_2O$, −78 °C, 2 h, 99%, for **10B**, 3-bromothiophene, *n*-BuLi, THF, −78 °C, 3 h, 24%, for **10C**, 2-bromopyridine, *i*-PrMgCl, THF, −40 °C, 12 h, 30%; (g) for **11A**: $H_2$, Pd/C, MeOH-THF, r.t., 18 h, 60%, for **11B**: $K_2CO_3$, MeOH, 80 °C, sealed tube, 3 d, 98%, for **11C**: TFA, DCM, r.t., 12 h, 99%; (h) **4**, $Pd_2(dba)_3$, BINAP, $NaO^tBu$, toluene, 130 °C, **12A** (48 h, 33%), **12B** (36 h, 35%), **12C** (12 h, 36%); (i) for **3A** and **3B**: $H_2$, Pd/C, MeOH, r.t., **3A** (2 h, 90%), **3B** (12 h, 98%), for **3C**: $BCl_3$, $C_6HMe_5$, DCM, 0 °C,15 min, 99%.

activities of **3I** with simple phenyl rings were almost as much as those of the piperidine analogue **3D**. However, the introduction of fluoro atoms in the two phenyl rings as in **3J** showed quite different results compared to non-fluoro compound **3I**. Suppression of most cancer cell proliferation with **3J** was retained to the level of the parent compound **2**. As can be seen in Fig. 3, among ten new derivatives, compounds **3A** and **3J** generally showed superior inhibition of proliferation in most cancer cell lines to other analogs. The growth inhibitory effects of **3A** and **3J** were better than compound **2** particularly in ARPC cell lines such as DU145 and PC-3.

To compare the growth inhibitory power of the compounds, **2**, **3A,** and **3J**, the concentration for 50% of maximal inhibition of cell proliferation ($IC_{50}$) was measured (Table 1). $IC_{50}$ values of **3A** and **3J** were a little higher in A549 and H1299 human lung cancer cell lines, but the values were lower in DU145 and PC-3 than the parent compound **2**. In case of LNCaP cell line, compounds **3A** and **3J** were a little bit better or equivalent to compound **2**. In the case of anticancer drug sunitinib, a multi-receptor tyrosine kinase inhibitor, $IC_{50}$ values against proliferation of DU145, PC-3, and LNCaP cell lines were 13.1, 15.5, and 20.8 μM, respectively. The results indicate that compounds **3A** and **3J** selectively inhibits ARPC proliferation.

We then checked how selective the inhibitory activities of the compounds against cancer cells compared to normal cells were by measuring the concentration for 50% of maximal cytotoxicity ($CC_{50}$) in three normal cell lines, CHO-KI, HEK-293, and CCD841 (Table 2). The $CC_{50}$ values of the three compounds, **2**, **3A,** and **3J**, were much higher than $IC_{50}$ values, and the $CC_{50}$ values between the three compounds were not so much different. In the case of sunitinib, the $CC_{50}$ values were observed 20.9, 7.3, 9.5 μM against CHO-K1, HEK-293, and CCD841, respectively [18].

To confirm an anticancer activity of the derivatives *in vivo*, we examined antitumor effects of **3A** and **3J** in chorioallantoic membrane (CAM) tumor model, in which DU145 cells were xenografted, and the effects of **3A** and **3J** were compared to that of the parent compound **2**. Compared to vehicle-treated controls, compounds **2, 3A** and **3J** suppressed tumor growth (Fig. 4Aa, 4B, 4C) and angiogenesis (Fig. 4Ab and 4C) in a dose-dependent manner.

### 2.3. Mechanism of action study

In order to search the possible molcular targets of compound **3A** showing a selective inhibitory effect on ARPC, we used the DeepZema® web server which is an interactive and integrated software system for accelerating drug discovery projects [19]. Firstly we predicted targets of compound **3A** by conformal prediction methods [20] which can be regarded as a new type of quantitavie structure activity relationship (QSAR) with information on the certainty of a prediction. Predicted targets of compound **3A** were M3R and M4R. The targets of compound **2** were also predicted to be M3R and M4R. Then compounds **2** and **3A** were docked into the binding site of rat M3R (PDB 5ZHP) using autodock vina [21] in order to understand protein–ligand binding interactions. Compound **3A** had a better docking score (−9.0 kCal/mol) than compound **2** (−8.1 kCal/mol). A proposed binding mode of compound **3A** to the rat M3R is shown in Fig. 5. Positively charged nitrogen

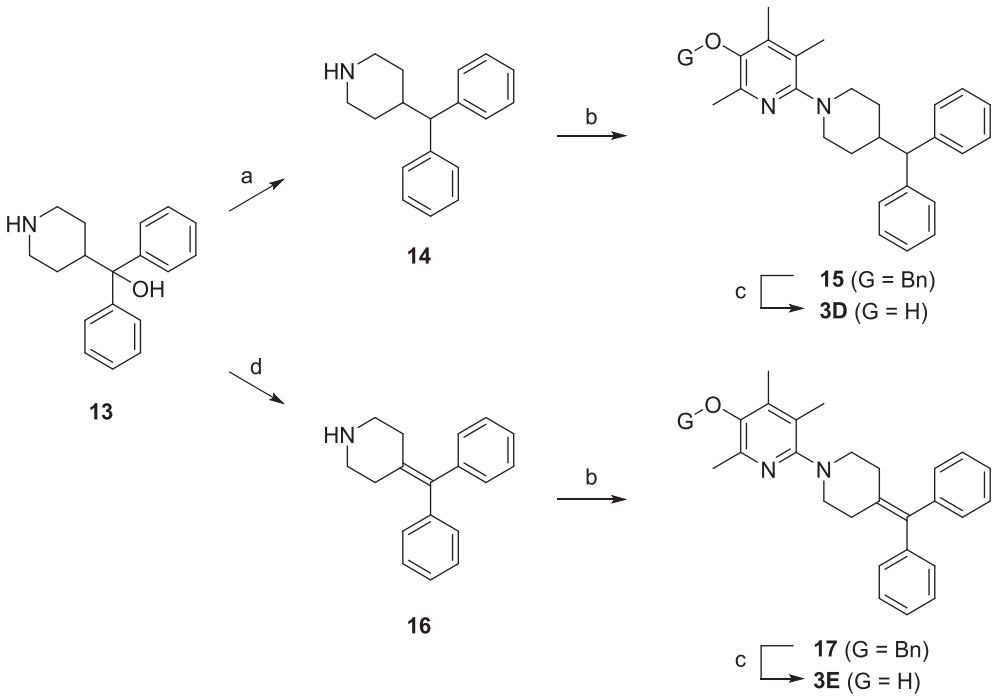


**Scheme 2.** Synthesis of compounds **3D** and **3E**. *Reagents and Conditions*: (a) $NaBH_4$, TFA, 0 °C, 50 min, 88%; (b) **4**, $Pd_2(dba)_3$, BINAP, $NaO^tBu$, toluene, 130 °C, **15** (20 h, 46%), **17** (12 h, 48%); (c) $H_2$, Pd/C, MeOH-$CHCl_3$, r.t., **3D** (6 h, 86%), **3E** (7 h, 14%); (d) TFA, DCM, r.t., 9 h, 95%.

atom of the pyridine ring forms a hydrogen bond to Tyr148, while the methyl groups contribute to the binding energy via hydrophobic interactions with residues with alkyl side chains such as Ile225, Leu225 and Val 510. The cyclohexyl and phenyl rings also make hydrophobic interactions.

In conjunction with the reports that ARPC expresses high levels of M1R and M3R [22], we performed a competitive M3R binding assay for compound **2** and **3A**, in which each compound competed with the binding of [$^3$H]-labeled 1,1-dimethyl-4-diphenylacetoxypiperidinium iodide (4-DAMP), a selective M3R antagonist [23], to M3R. In the competitive binding assay, compound **3A** showed $K_i = 1$ μM and $IC_{50} = 1.4$ μM (Fig. 6). However, $IC_{50}$ of compound **2** was greater than >10 μM and $K_i$ was not calculable because higher concentrations of compound **2** could not be prepared for the assay due to solubility problem. The results indicate that compound **3A** was more than seven fold potent than compound **2** in inhibiting the binding of [$^3$H]4-DAMP, although binding affinity of compound **3A** to M3R is relatively low.

We, then, compared the inhibitory effects of compounds **2** and **3A** on carbachol-induced proliferation of DU145 cells. Treatment of DU145 cells with carbachol in the presence of low level serum (1%) induced a minimal level increase in cell proliferation (Fig. 7A). This might be because the proliferative action of serum counteracts the effect of carbachol. The carbachol and serum (1%)-induced proliferation was concentration dependently inhibited by compounds **2** (Fig. 7B) and **3A** (Fig. 7C), and the inhibitory effect of compound **3A** was much stronger than that of compound **2**. In the absence of serum, carbachol increased cell survival in a concentration- and time-dependent manner (Fig. 7D). The carbachol (300 μM) alone-induced viability of DU145 cells was inhibited by compounds **2** and **3A**, and compound **3A** was more potent than compound **2** (Fig. 7E). These results support that action of compound **3A** in enhancing viable number of DU145 cells was mediated through M3R.

We also compared the inhibitory effects of compounds **2**, **3A**, and **3J** on carbachol-induced NOX activity, based on the reports that GPCR is linked to NOX activation [24], and carbachol, a muscarinic receptor agonist, increases NOX-dependent ROS (Fig. 8) [25]. Compounds **2**, **3A**, and **3J** concentration-dependently inhibited carbachol (300 μM)-induced NOX activity. The inhibitory activity of compound **3A** was the best and much stronger than that of VAS2870, a NOX2/4 inhibitor, which also showed concentration-dependent inhibitory effect on carbachol-induced NOX activity. Compound **3J** which showed the lowest inhibitory activity was almost similar to that of VAS2870. The results implicate that compounds **2** and **3A** have similar target, M3R, which might not be the case for compound **3J**.

## 3. Conclusion

In the current study, we found that anti-proliferative activity of compound **3A** was better than the parent compound, 6-azacyclonol-2,4,6-trimethylpyridin-3-ol, particularly in ARPC cell line. The results from molecular docking, competitive receptor binding assay, and carbachol-induced cell viability and NOX activation indicate that ARPC-selective activity of compound **3A** was associated with its antagonistic action to M3R which is highly expressed in ARPC and serves as a prostate cancer progression marker. Based on the structure of compound **3A**, it may be possible to design and develop anticancer compounds with high affinity and selectivity to M3R for the treatment of ARPC which overexpresses the receptor. However, M1R is also upregulated in patient tissues and cell lines of ARPC [4,6], and plays a role in the proliferation, migration, and invasion of prostate cancers [4]. A previous study has focused on targeting the common signaling pathways of M1R and M3R which are involved in ARPC progression [6]. From the current study, we propose that it may be possible to develop an ARPC therapeutic agent that simultaneously inhibits both M1R and M3R through rational chemical modification of compound **3A**.

## 4. Experimental section

### 4.1. Synthesis [26]

#### 4.1.1. General

Unless noted otherwise, materials were purchased from commercial suppliers and used without further purification. Air or moisture-sensitive reactions were carried out under an inert gas atmosphere.

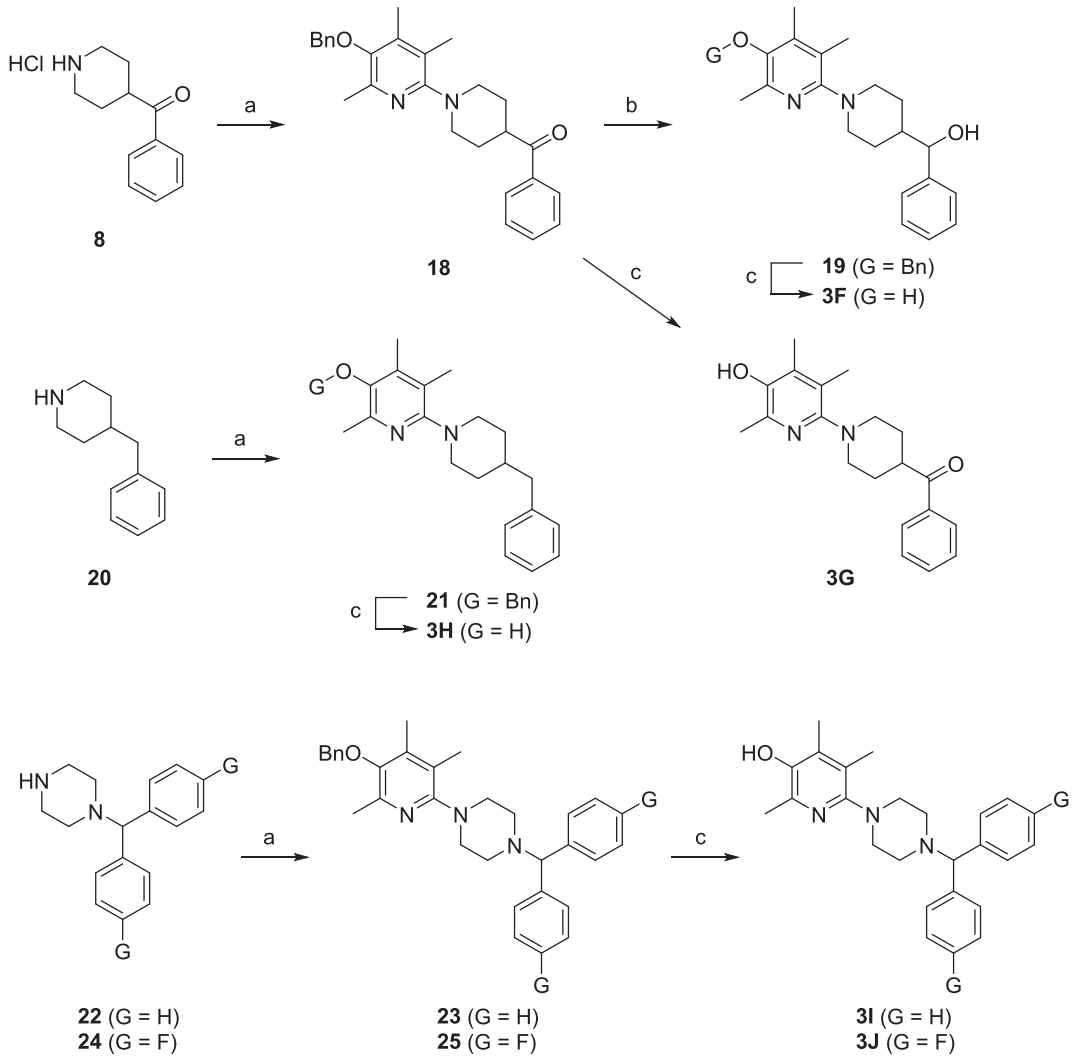


**Scheme 3.** Synthesis of compounds **3F**–**3J**. *Reagents and Conditions*: (a) **4**, $Pd_2(dba)_3$, BINAP, NaO$^t$Bu, toluene, 130 °C, **18** (24 h, 27%), **21** (3 h, 72%), **23** (3 h, 56%), **25** (5 h, 41%); (b) $NaBH_4$, MeOH-$H_2O$, r.t., 30 min, 99%; (c) for **3F**–**3H**: $H_2$, Pd/C, MeOH-$CHCl_3$, r.t., **3F** (2 h, 77%), **3G** (1.5 h, 76%), **3H** (3 h, 95%), for **3I**: $BCl_3$, $C_6HMe_5$, DCM, 0 °C, 30 min, 87%, for **3J**: $H_2$, Pd/C, MeOH, r.t., 3 h, 95%.

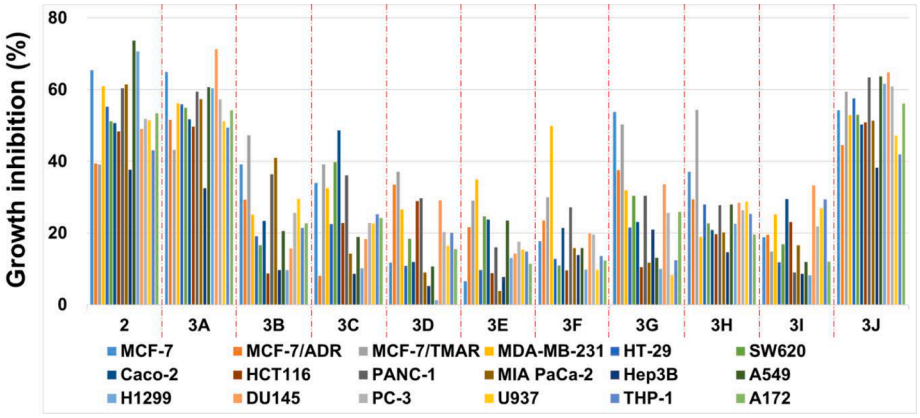


**Fig. 3.** Bar graph showing the mean percentage inhibition of each compound at 30 μM concentration against eighteen cancer cell proliferation.

The reaction progress was monitored by thin layer-chromatography (TLC) using silica gel $F_{254}$ plates. The products were purified by flash column chromatography using silica gel 60 (70–230 mesh) or by using the Biotage 'Isolera One' system with indicated solvents. Melting points were determined using a Fisher–Johns melting point apparatus and were not corrected. Low-resolution mass spectra (LRMS) were obtained using a Jeol ColdSpray-LC-TOF-MS and recorded in a positive ion mode with an electrospray (ESI) source. NMR spectra were obtained using a Bruker-250 spectrometer (250 MHz for $^1$H NMR and 62.5 MHz for $^{13}$C NMR) and a Bruker Avance Neo 400 spectrometer (400 MHz for $^1$H NMR).

**Table 1**
$IC_{50}$ of the selected compounds against proliferation of human cancer cell lines.

| Cancer cell line | $IC_{50}$ (μM)[a] | | |
|---|---|---|---|
| | **2** | **3A** | **3J** |
| MCF-7 | 10.9 ± 1.0 | 11.9 ± 1.5 | 17.0 ± 2.7 |
| MCF-7/ADR | 33.2 ± 3.2 | 29.0 ± 3.4 | 31.9 ± 3.7 |
| MCF-7/TMAR | 29.3 ± 2.7 | 22.2 ± 2.4 | 18.4 ± 1.5 |
| MDA-MB-231 | 14.7 ± 1.8 | 18.6 ± 2.6 | 21.7 ± 2.9 |
| HT-29 | 18.6 ± 0.8 | 17.8 ± 1.3 | 20.6 ± 2.3 |
| SW620 | 24.3 ± 2.0 | 27.9 ± 1.8 | 25.0 ± 1.7 |
| Caco-2 | 28.6 ± 1.2 | 29.6 ± 3.9 | 25.4 ± 1.4 |
| HCT116 | 29.1 ± 1.7 | 30.6 ± 2.0 | 29.2 ± 1.9 |
| PANC-1 | 21.9 ± 3.5 | 16.0 ± 1.3 | 14.2 ± 1.3 |
| MIA PaCa-2 | 18.2 ± 2.9 | 18.8 ± 2.0 | 24.8 ± 2.7 |
| Hep3B | 31.6 ± 2.8 | 64.1 ± 3.6 | 35.5 ± 1.0 |
| A549 | 8.2 ± 0.7 | 15.0 ± 1.9 | 12.4 ± 1.5 |
| H1299 | 11.0 ± 1.4 | 14.8 ± 2.2 | 14.3 ± 1.8 |
| DU145 | 18.3 ± 2.2 | 1.7 ± 0.1 | 5.0 ± 0.3 |
| PC-3 | 26.5 ± 4.4 | 11.3 ± 3.8 | 13.3 ± 2.4 |
| LNCaP | 51.6 ± 2.4 | 45.5 ± 1.4 | 50.8 ± 2.8 |
| U937 | 31.8 ± 2.3 | 28.8 ± 2.6 | 33.0 ± 2.2 |
| THP-1 | 41.0 ± 3.0 | 33.1 ± 2.6 | 39.1 ± 3.3 |
| A172 | 25.4 ± 1.7 | 29.2 ± 1.9 | 23.8 ± 1.3 |

[a] The values are mean ± SEM of three independent experiments performed in triplicate.

**Table 2**
$CC_{50}$ of the selected compounds against normal cell lines.

| Normal cell line | $CC_{50}$ (μM)[a] | | |
|---|---|---|---|
| | **2** | **3A** | **3J** |
| CHO-K1 | 67.6 ± 1.3 | 69.1 ± 2.1 | 63.1 ± 4.3 |
| HEK 293 | 61.7 ± 1.2 | 76.9 ± 2.4 | 72.4 ± 3.0 |
| CCD 841 | 69.2 ± 3.8 | 75.8 ± 3.1 | 70.2 ± 2.8 |

[a] The values are mean ± SEM of three independent experiments performed in triplicate.

Chemical shifts (δ) were expressed in ppm using a solvent as an internal standard and the coupling constant (J) in hertz. HPLC analyses were performed on a system consisted of an LC-20AD pump, a CBM-20A communication bus module, an SPD-20A UV–visible detector, and a DGU-20A5 degasser from Shimadzu Corporation (Kyoto, Japan). A Phenomenex Luna C18 column (250 × 4.6 mm, 5.0 μm) (Torrance, CA, USA) was used with a gradient solvent system consisted of acetonitrile and water (from 30% to 100% of acetonitrile over 20 min, then 100% of acetonitrile for 10–20 min) at a flow rate of 1.0 mL/min at 254 nm UV detection. Purity of compound was recorded as a percentage (%) and retention time was given in minutes.

#### *4.1.2. Benzyl 4-benzoylpiperidine-1-carboxylate (**9–1**) [CAS RN 922504-27-6]*

To a mixture of 4-benzoylpiperidine hydrochloride (**8**, 3.0 g, 13.29 mmol) in THF (40 mL) were successively added potassium carbonate (5.5 g, 39.80 mmol), THF (40 mL), and benzyl chloroformate (2.1 mL, 15.28 mmol) at 0 °C. The mixture was brought to room temperature slowly and was stirred for 2 h. DCM was added to it and was washed thrice with brine. It was dried over $MgSO_4$, filtered and concentrated to get **9-1** (3.8 g, 90% yield) as a colorless oil. $R_f$ 0.50 (DCM:MeOH = 20:1); $^1$H NMR ($CDCl_3$) δ 7.98–7.90 (m, 2H), 7.62–7.43 (m, 3H), 7.41–7.28 (m, 5H), 5.15 (s, 2H), 4.24 (d, *J* = 12.9 Hz, 2H), 3.50–3.37 (m, 1H), 3.00 (t, *J* = 12.4 Hz, 2H), 1.97–1.63 (m, 4H).

#### *4.1.3. Benzyl 4-(cyclohexyl(hydroxy)(phenyl)methyl)piperidine-1-carboxylate (**10A**)*

In a flame-dried round bottomed flask, **9-1** (600 mg, 1.80 mmol) was added at −78 °C. Dry ethyl ether (18 mL) was added to it followed by the dropwise addition of cyclohexylmagnesium bromide (2 M, 2.8 mL, 5.58 mmol). The mixture was stirred for 2 h maintaining anhydrous condition at −78 °C. After completion of the reaction, it was quenched with aqueous $NH_4Cl$ and extracted with EtOAc. The EtOAc layer was dried over $MgSO_4$ and concentrated to get **10A** (727 mg, 99% yield) as a white solid. $R_f$ 0.50 (DCM:MeOH = 20:1); m.p. 132 °C; MS *m/z* 408.28 $[M + H]^+$; $^1$H NMR ($CDCl_3$) δ 7.42–7.26 (m, 10*H*), 5.07 (s, 2H), 4.21 (s, 2H), 2.73 (q, *J* = 12.7 Hz, 2H), 2.06 (d, *J* = 11.9 Hz, 1H), 1.96–1.65 (m, 8H), 1.53–1.37 (m, 2H), 1.32–1.12 (m, 4H), 1.08–0.82 (m, 4H); $^{13}$C NMR ($CDCl_3$) δ 155.09, 142.82, 136.89, 128.41(2C), 127.85, 127.73(2C), 127.64(2C), 126.46, 126.26(2C), 79.97, 66.89, 44.34(2C), 42.45, 35.54, 27.33, 26.71, 26.57, 26.51, 26.45(2C), 24.13.

#### *4.1.4. Cyclohexyl(phenyl)(piperidin-4-yl)methanol (**11A**) [CAS RN 64061-56-9]*

To a solution of **10A** (145 mg, 0.35 mmol) in MeOH-THF (1:1, 10 mL) was added 10% palladium on carbon (37 mg, 0.035 mmol). The mixture was stirred under hydrogen atmosphere at room temperature for 18 h. The mixture was filtered through Celite pad and the filtrate was concentrated to give **11A** (58 mg, 60% yield) as a white solid. $R_f$ 0.20 (DCM:MeOH = 9:1); $^1$H NMR ($CDCl_3$) δ 7.39–7.17 (m, 5H), 3.17 (dd, *J* = 24.8, 12.1 Hz, 2H), 2.63 (ddd, *J* = 17.9, 12.3, 8.1 Hz, 2H), 2.11 (dd, *J* = 8.7, 5.7 Hz, 1H), 1.92–1.66 (m, 6H), 1.25 (ddd, *J* = 12.9, 11.2, 3.9 Hz, 6H), 1.06–0.80 (m, 2H), 0.75–0.58 (m, 1H).

#### *4.1.5. (1-(5-(Benzyloxy)-3,4,6-trimethylpyridin-2-yl)piperidin-4-yl)(cyclohexyl)(phenyl)methanol (**12A**)*

3-(Benzyloxy)-6-bromo-2,4,5-trimethylpyridine (**4**, 50 mg, 0.17 mmol) was taken in a round-bottomed flask and to it were added tris (dibenzylideneacetone)dipalladium(0) (4 mg, 0.003 mmol), 2,2′-bis (diphenylphosphino)-1,1′-binaphthyl (4 mg, 0.006 mmol), sodium *tert*-butoxide (13 mg, 0.13 mmol), **11A** (55 mg, 0.20 mmol), and anhydrous toluene (5 mL). The reaction mixture was refluxed for 48 h. After cooling, brine and EtOAc were added to the mixture and was then washed several times with brine. The EtOAc layer was dried with $MgSO_4$, filtered, and concentrated. The residue was purified by silica gel column chromatography (EA:HX = 1:8) to give **12A** (28 mg, 33% yield) as a white solid. $R_f$ 0.30 (EA:HX = 1:5); m.p. 130 °C; MS *m/z* 499.38 $[M + H]^+$; $^1$H NMR ($CDCl_3$) δ 7.53–7.29 (m, 10*H*), 4.73 (s, 2H), 3.28 (dd, *J* = 22.5, 12.3 Hz, 2H), 2.77 (d, *J* = 9.3 Hz, 2H), 2.42 (s, 3H), 2.12 (d, *J* = 19.3 Hz, 6H), 1.90 (d, *J* = 9.1 Hz, 2H), 1.78–1.57 (m, 6H), 1.52–1.42 (m, 2H), 1.02–0.68 (m, 6H); $^{13}$C NMR ($CDCl_3$) δ 157.82, 147.78, 146.05, 143.27, 140.24, 137.36, 128.53(2C), 128.05, 127.85 (2C), 127.51(2C), 126.41(2C), 126.24, 122.69, 80.14, 74.71, 51.33, 51.22, 44.39, 42.32, 29.69, 27.42, 26.95, 26.80, 26.74, 26.63, 26.49, 26.29, 19.26, 14.43, 13.02.

#### *4.1.6. 6-(4-(Cyclohexyl(hydroxy)(phenyl)methyl)piperidin-1-yl)-2,4,5-trimethylpyridin-3-ol (**3A**)*

To a solution of **12A** (25 mg, 0.05 mmol) in MeOH (4 mL) was added 10% palladium on carbon (5 mg, 0.005 mmol). The mixture was stirred under hydrogen atmosphere at room temperature for 2 h, and the mixture was filtered through Celite pad. The filtrate was concentrated to get **3A** (18 mg, 90% yield) as a white solid. $R_f$ 0.30 (DCM:MeOH = 20:1); m.p. 108 °C; MS *m/z* 409.3 $[M + H]^+$; $^1$H NMR ($CD_3OD$) δ 7.90 (s, 1H), 7.42 (d, *J* = 7.4 Hz, 2H), 7.33 (dd, *J* = 13.5, 6.2 Hz, 2H), 7.22 (t, *J* = 7.3 Hz, 1H), 3.28–3.15 (m, 2H), 2.93 (dd, *J* = 26.4, 13.1 Hz, 2H), 2.40 (s, 3H), 2.23 (d, *J* = 7.5 Hz, 3H), 2.14 (s, 3H), 1.99–1.90 (m, 3H), 1.74 (t, *J* = 14.7 Hz, 2H), 1.67–1.49 (m, 4H), 1.40–1.20 (m, 4H), 1.11–0.98 (m, 2H), 0.77 (dd, *J* = 12.6, 3.0 Hz, 1H); $^{13}$C NMR ($CDCl_3$) δ 142.73, 127.57 (2C), 126.35(2C), 124.98, 80.14, 51.37(2C), 44.45(2C), 41.67, 27.40, 26.74 (2C), 26.59, 26.42, 26.27, 16.78, 14.43, 13.57; HPLC retention time 17.6 min, purity 97.7%.

#### *4.1.7. 1-(5-(Benzyloxy)-3,4,6-trimethylpyridin-2-yl)-4-(bis(4-fluorophenyl)methyl)piperazine (**25**)*

To a mixture of 3-(benzyloxy)-6-bromo-2,4,5-trimethylpyridine (**4**,

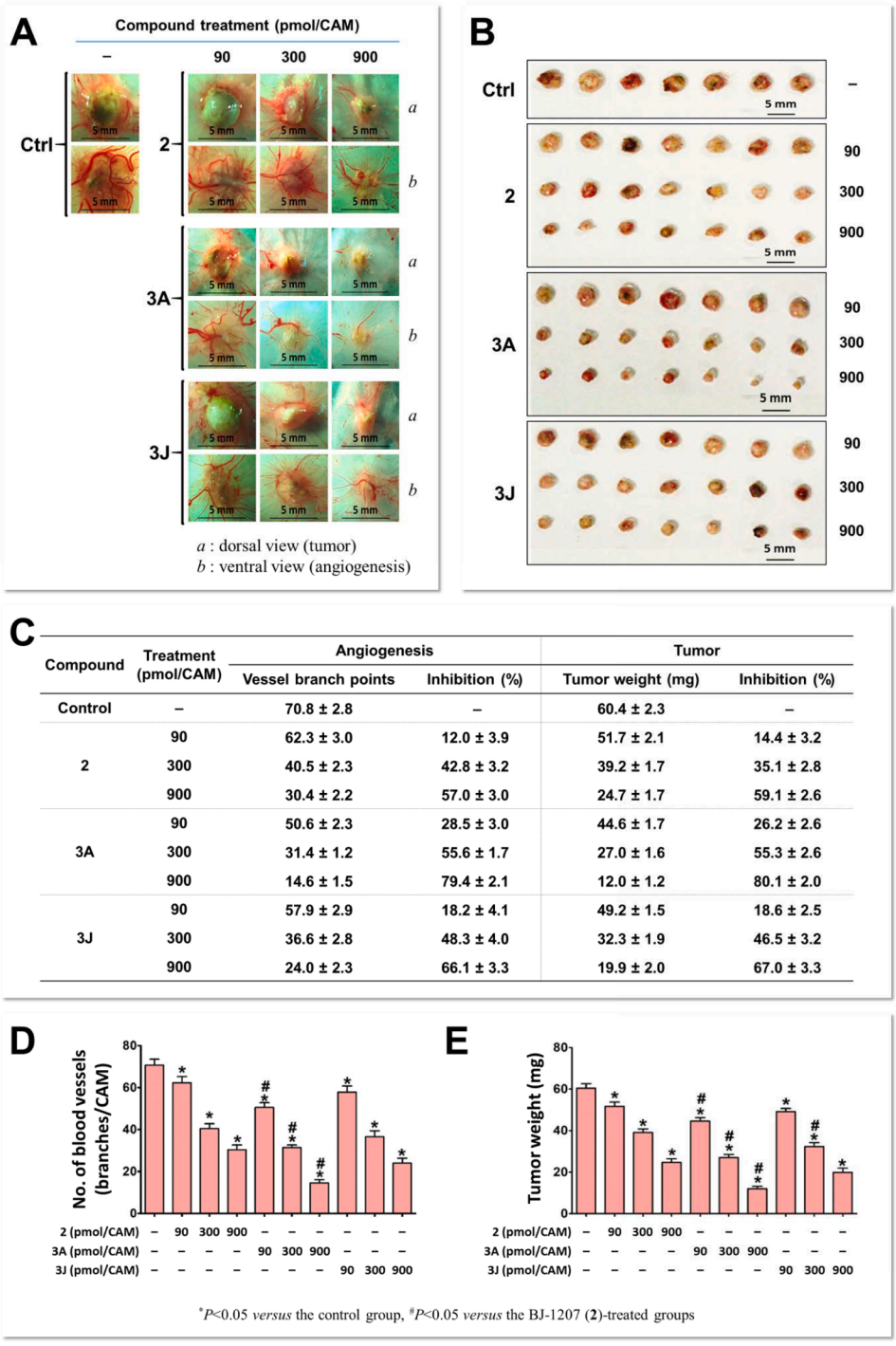


C

| Compound | Treatment (pmol/CAM) | Angiogenesis | | Tumor | |
|---|---|---|---|---|---|
| | | Vessel branch points | Inhibition (%) | Tumor weight (mg) | Inhibition (%) |
| Control | – | 70.8 ± 2.8 | – | 60.4 ± 2.3 | – |
| 2 | 90 | 62.3 ± 3.0 | 12.0 ± 3.9 | 51.7 ± 2.1 | 14.4 ± 3.2 |
| | 300 | 40.5 ± 2.3 | 42.8 ± 3.2 | 39.2 ± 1.7 | 35.1 ± 2.8 |
| | 900 | 30.4 ± 2.2 | 57.0 ± 3.0 | 24.7 ± 1.7 | 59.1 ± 2.6 |
| 3A | 90 | 50.6 ± 2.3 | 28.5 ± 3.0 | 44.6 ± 1.7 | 26.2 ± 2.6 |
| | 300 | 31.4 ± 1.2 | 55.6 ± 1.7 | 27.0 ± 1.6 | 55.3 ± 2.6 |
| | 900 | 14.6 ± 1.5 | 79.4 ± 2.1 | 12.0 ± 1.2 | 80.1 ± 2.0 |
| 3J | 90 | 57.9 ± 2.9 | 18.2 ± 4.1 | 49.2 ± 1.5 | 18.6 ± 2.5 |
| | 300 | 36.6 ± 2.8 | 48.3 ± 4.0 | 32.3 ± 1.9 | 46.5 ± 3.2 |
| | 900 | 24.0 ± 2.3 | 66.1 ± 3.3 | 19.9 ± 2.0 | 67.0 ± 3.3 |




*$P$<0.05 *versus* the control group, #$P$<0.05 *versus* the BJ-1207 (**2**)-treated groups

**Fig. 4.** Effect of compounds, **2**, **3A,** and **3J** on tumor growth in DU145-xenografted CAM tumor model. (A, B) Comparison of inhibitory effects of compounds, **2**, **3A,** and **3J** on DU145-induced angiogenesis (A, scale bars, 5 mm) and tumor size (B). The images of angiogenesis are representative of each group. The control CAM was exposed to the vehicle. (C-E) Quantitation of angiogenesis and tumor size. The quantitation of new branches formed from existing blood vessels and weighing of tumors grown on the CAM were performed five days after cancer cell implantation. Data are presented as the mean ± standard deviation from seven different samples. *$P < 0.05$ vs. vehicle-treated control. #$P < 0.05$ vs. compound **2** or **3J**-treated group.

100 mg, 0.33 mmol), 1-(bis(4-fluorophenyl)methyl)piperazine (**24**, 94 mg, 0.33 mmol) in toluene (5 mL) were added tris(dibenzylideneacetone)dipalladium(0) (7 mg, 0.007 mmol), 2,2′-bis(diphenylphosphino)-1,1′-binaphthyl (8 mg, 0.013 mmol), and sodium *tert*-butoxide (44 mg, 0.44 mmol). The mixture was refluxed for 5 h and cooled to room temperature. EtOAc and brine were added to the mixture and the organic layer was washed with brine several times. The organic solution was dried over $MgSO_4$, filtered, and concentrated. The residue was purified by silica gel column chromatography (EA:HX = 1:10) to give **25** (68 mg, 41% yield) as a pale yellow solid. $R_f$ 0.30 (Hx:EA = 5:1); m.p. 118 °C; MS *m/z* 514.29 $[M + H]^+$; $^1H$ NMR ($CDCl_3$) $\delta$ 7.50–7.33 (m, 9H), 6.98 (t, $J$ = 8.7 Hz, 4H), 4.74 (s, 2H), 4.31 (s, 1H), 3.11–3.02 (m, 4H), 2.52 (s, 4H), 2.43 (s, 3H), 2.17 (s, 3H), 2.12 (s, 3H); $^{13}C$ NMR ($CDCl_3$) $\delta$ 163.75, 159.86, 157.10, 147.99, 146.31(2C), 140.42, 138.40, 137.30, 129.36, 129.24, 128.67, 128.55 (2C), 128.09, 127.98, 127.86 (2C), 122.49, 115.53 (2C), 115.19 (2C), 74.75, 74.52, 52.05 (2C), 50.46 (2C), 19.29, 14.41, 13.03.

#### *4.1.8. 6-(4-(Bis(4-fluorophenyl)methyl)piperazin-1-yl)-2,4,5-trimethylpyridin-3-ol (**3J**)*

To a solution of **25** (40 mg, 0.07 mmol) in methanol (5 mL) was added 10% palladium on carbon (7 mg, 0.007 mmol). The mixture was stirred under hydrogen atmosphere at room temperature for 3 h then filtered through Celite pad. The filtrate was concentrated to give **3J** (28

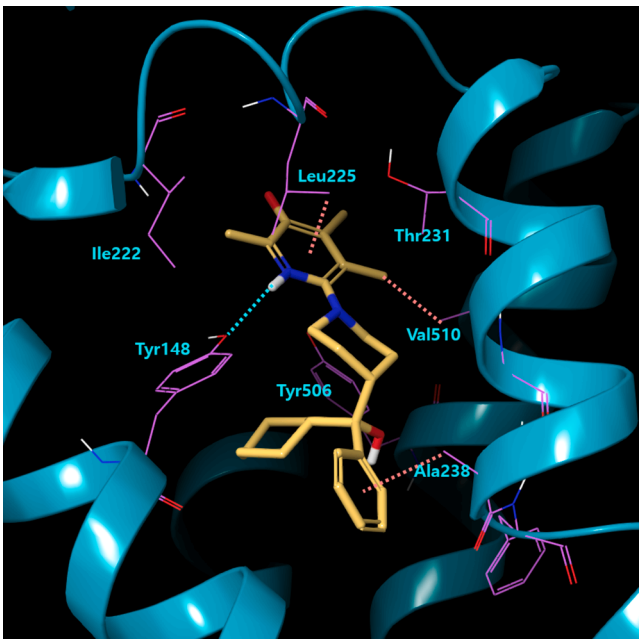


**Fig. 5.** Binding mode of M3R-compound **3A** complex.

mg, 95% yield) as a white solid. $R_f$ 0.25 (EA:Hx = 1:5); m.p. 89 °C; MS *m/z* 424.25 $[M + H]^+$; $^1H$ NMR ($CDCl_3$) $\delta$ 7.38 (dd, $J$ = 8.3, 5.6 Hz, 4H), 6.98 (t, $J$ = 8.5 Hz, 4H), 4.36 (s, 1H), 4.30 (s, 1H), 3.07–2.92 (m, 4H), 2.50 (s, 4H), 2.39 (s, 3H), 2.14 (s, 6H); $^{13}C$ NMR ($CD_3OD$) $\delta$ 163.78, 159.90, 154.06, 145.68, 140.41, 138.64, 138.59, 135.53, 129.34(2C), 129.21(2C), 123.14, 114.93(2C), 114.59(2C), 74.60, 52.13(2C), 50.20 (2C), 17.34, 12.90, 11.38; HPLC retention time 19.5 min, purity 98.2%.

### 4.2. Biological evaluation

#### 4.2.1. Cell lines and culture

Seventeen human cancer cell lines derived from breast (MCF-7, MDA-MB-231), colon (HT-29, SW620, Caco-2, HCT-116), pancreas (PANC-1, MiaPaCa-2), liver (Hep3B), lung (A549, H1299), prostate (DU-145, PC-3, LNCaP), blood (U937, TPH-1), and brain (A172) were obtained from American Type Culture Collection (ATCC, USA) and Korean Cell Line Bank (KCLB). Adriamycin-resistant and tamoxifen-resistant MCF cell lines, MCF-7/ADR and MCF-7/TAMR, respectively, were generously provided by Prof. Keon Wook Kang (Seoul National University, College of Pharmacy). Normal human colon epithelial cell line CCD841 was obtained from ATCC, and two normal cell lines, CHO-K1 (Chinese hamster ovary cell line) and HEK-293 (human embryonic kidney cell line), were obtained from KCLB. The cells were cultured in standard growth medium supplemented with 10% fetal bovine serum (FBS), 1% penicillin/streptomycin and incubated at 37 °C under a 5% $CO_2$ atmosphere.

#### 4.2.2. Cell proliferation assay

Cells were seeded at a density of 5000 cells/well in a 96-well plate. After overnight incubation, the cells were serum-starved using 1% FBS. The next day, the cells were pre-treated with the indicated concentrations of drugs for 1 h prior to the treatment with serum (10% FBS). After 72 h of incubation, 3-(4,5-dimethylthiazol-2-yl)-2,5-diphenyltetrazolium bromide (MTT) dye solution was added and incubated for 4 h. Next, DMSO was added, and after 30 min, the color intensities were measured using a microplate reader (Versamax, Molecular Devices, Inc., USA) at 490 nm.

#### 4.2.3. Cytotoxicity assay

The cytotoxicity of the compounds was assessed by measuring the cell viability decrease using the MTT staining method. Briefly, cells were seeded in a 96-well plate (Falcon, USA) at a density of $1 \times 10^4$ cells per well. The next day, culture medium was changed into 1% serum containing medium, and cells were incubated with different concentrations of each compound for 24 h. Then, 10 μL of MTT solution was added to the well and further incubated for 4 h at 37 °C. At the end of the incubation, the media were removed, and 200 μL of dimethyl sulfoxide (DMSO) was added into each well to solubilize the formazan crystals. Finally, the absorbance was measured at 540 nm using a microplate reader (Molecular Devices, Versa MAX Sunnyvale, CA, USA).

#### 4.2.4. NOX activity measurement

NOX activity was assayed with lucigenin method as previously reported [11] with some modification. In short, cells were washed thoroughly with ice cold 1x Phosphate-buffered saline (PBS) and collected in Krebs-HEPES buffer of pH 7.4 (118 mM NaCl, 4 mM KCl, 2.5 mM $CaCl_2$, 1.18 mM $MgSO_4$, 1.18 mM $KH_2PO_4$, 24.9 mM $NaHCO_3$, 11 mM glucose, 0.03 mM EDTA, and 20 mM HEPES) containing protease and phosphatase inhibitors (Thermo Scientific, Rockford, IL, USA). Cells were then homogenized with Dounce homogenizer and protein concentration was determined using BCA protein assay kit (Thermo Scientific). The chemiluminescence was measured using a FLUOstar Optima microplate reader (BMG LABTECH) immediately after adding 50 μg protein to each well containing mixture of test compounds (3, 10, and 30 μM), lucigenin (5 μM), NADPH (100 μM) and inducer (10% FBS or 300 μM carbachol).

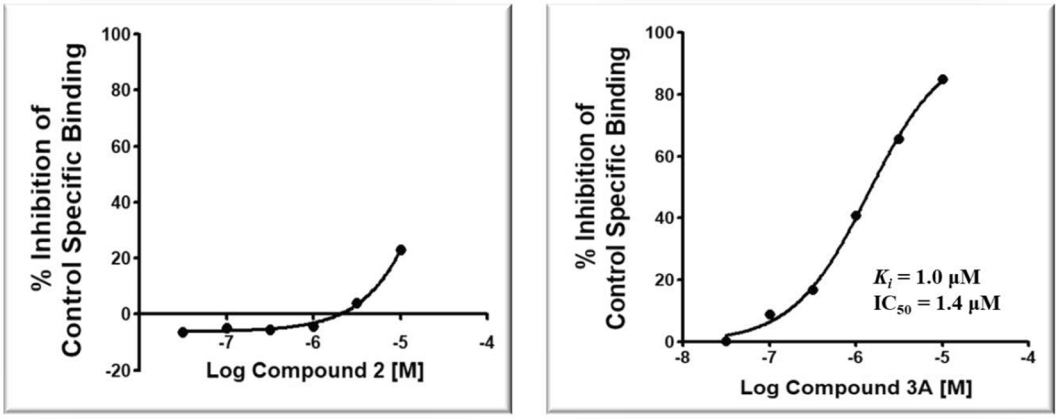


**Fig. 6.** Competition binding assay of compounds **2** and **3A** for $[^3H]$4-DAMP binding sites in human recombinant M3R which were expressed in CHO cells. $K_i$ and $IC_{50}$ were calculated as described in Experimental Section.

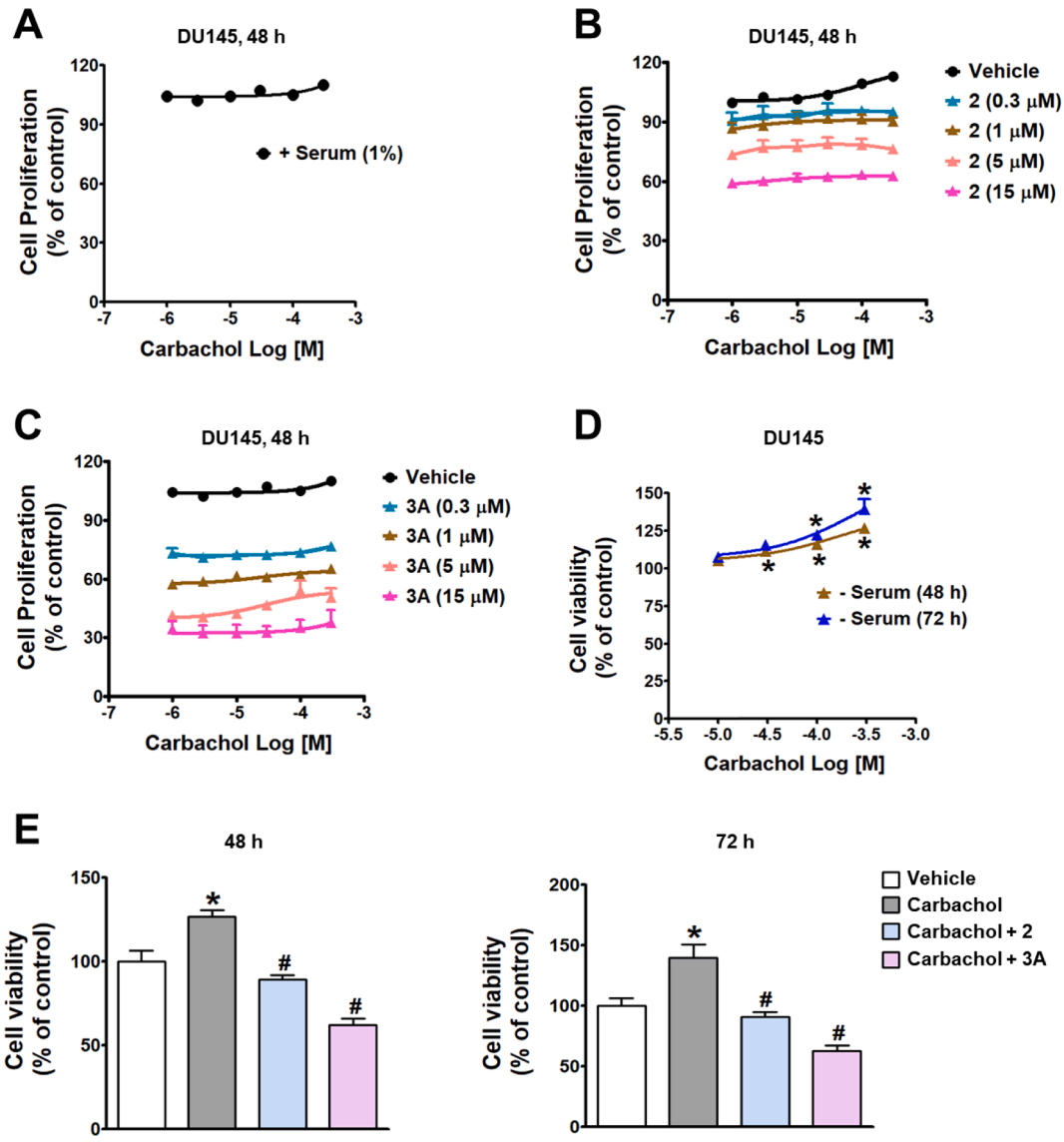


**Fig. 7.** The inhibitory effects of compound **3A** on carbachol-induced DU145 cell proliferation and survival. (A) DU145 cells were treated with different concentrations of carbachol in the presence of low level serum (1%). (B, C) DU145 cells were treated with increasing concentrations of compound **2** or **3A** with different concentrations of carbachol in the presence of 1% serum. (D) DU145 cells were treated with increasing concentrations of carbachol alone in the absence of serum for 48 or 72 h. (E) DU145 cells were co-treated with 300 μM carbachol and 10 μM of compound **2** or **3A** for 48 or 72 h. $^{*}P < 0.05$ versus the vehicle-treated control group. $^{\#}P < 0.05$ versus carbachol-treated group.

*4.2.5. CAM (chick chorioallantoic membrane) tumor model*

Fertile chicken eggs were purchased from Byeolbichon Farm (Gyeongbuk, South Korea) and incubated at 37 °C and under 55% relative humidity. On the 9th day of egg incubation (post-fertilization), false air sac was generated on the relatively flat side of eggs by a negative pressure technique. A small window (1 $cm^2$) was created on the false air sac surface of the eggs by separating the shell and membrane beneath (technique) using a grinding wheel (Dremel, Racine, WI, USA). Next, DU145 cells were loaded at a density of $1.5 \times 10^6$ cells/CAM with or without compound. After five days of drug treatment, the tumor weight, number of vessel branch points within the tumor region were analyzed.

The chick embryo experiments were approved beforehand by the Institutional Animal Care and Use Committee of Yeungnam University and were performed accordingly the guidelines issued by the Institute of Laboratory Animal Resources (1996) and Yeungnam University (The care and use of animals 2009).

*4.2.6. Radioligand binding assay*

Competitive M3R binding assay was performed in the laboratory of Eurofins Discovery (France). Briefly, human recombinant M3R overexpressed in CHO cells were incubated with 0.2 nM [$^3$H]4-DAMP and serial dilutions of compounds **2** and **3A** for 1 hr at room temperature. Nonspecific binding was determined in the presence of 1 μM atropine. The results were expressed as a percent inhibition of control specific binding in the presence of the test compounds. Concentration causing a half-maximal inhibition of control specific binding ($IC_{50}$) and Hill coefficients (nH) were determined by non-linear analysis of the competition curves generated with mean replicate values using Hill equation curve fitting. The inhibition constant ($K_i$) was calculated using the Cheng Prusoff equation.

*4.2.7. Carbachol-induced DU145 cell survival assay*

DU145 cells were seeded in 96-well plates at a density 5000 cells/well using complete (10% FBS containing) media and incubated for 24 h. Then, cells were washed three times with warm Hank's balanced salt

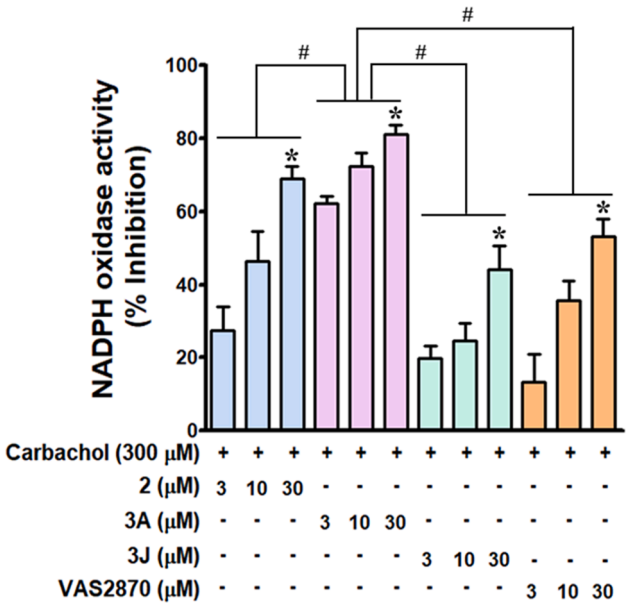


**Fig. 8.** Inhibitory effects of compounds **2**, **3A,** and **3J** on carbachol-induced NOX activity. NOX activity was measured by lucigenin-dependent chemiluminescence using DU145 cell extracts as an NOX enzyme source. $^{*}P < 0.05$ versus 3 μM-treated group in each compound. $^{\#}P < 0.05$ versus the same concentration of compounds.

solution and treated with different concentrations of carbachol in the absence of serum for 48 or 72 h. In case of comparison of the inhibitory effects of compounds, cells were treated with 300 μM carbachol with 10 μM compounds in serum-free culture medium for 48 or 72 h. After that, MTT assay was performed and absorbance was measured at 540 nm using a SPECTROStar Nano microplate reader (BMG LABTECH).

#### *4.2.8. Statistical analysis*

The results are presented as the mean ± S.E.M. and were analyzed using one-way ANOVA followed by the Newman-Keuls comparison method using the GraphPad Prism software (version 5.0) (San Diego, CA, USA). *P* values less than 0.05 were considered statistically significant.

## Declaration of Competing Interest

The authors declare that they have no known competing financial interests or personal relationships that could have appeared to influence the work reported in this paper.

## Acknowledgements

This work were supported by the National Research Foundation of Korea (NRF) grants funded by the Korea government (MIST) (No. NRF-2018R1A2B6001299 and NRF-2020R1A2C2005690).

## Appendix A. Supplementary material

Supplementary data to this article can be found online at https://doi.org/10.1016/j.bioorg.2021.104805.

## References

[1] F. Bray, J. Ferlay, I. Soerjomataram, R.L. Siegel, L.A. Torrre, A. Jemal, Global cancer statistics 2018: GLOBOCAN estimates of incidence and mortality worldwide for 36 cancers in 185 countries, CA Cancer J. Clin. 68 (2018) (2018) 394–424.

[2] M. Nakazawa, C. Paller, N. Kyprianou, Mechanisms of therapeutic resistance in prostate cancer, Curr. Oncol. Rep. 19 (2017) 13.

[3] G.R. Luthin, P. Wang, H. Zhou, D. Dhanasekaran, M.R. Ruggieri, Role of m1 receptor-G protein coupling in cell proliferation in the prostate, Life Sci. 60 (1997) 963–968.

[4] Q.Q. Yin, L.H. Xu, M. Zhang, C. Xu, Muscarinic acetylcholine receptor M1 mediates prostate cancer cell migration and invasion through hedgehog signaling, Asian J Androl. 20 (2018) 608–614.

[5] N. Wang, M. Yao, J. Xu, Y. Quan, K. Zhang, R. Yang, W.-Q. Gao, Autocrine activation of CHRM3 promotes prostate cancer growth and castration resistance via CaM/CaMKK-mediated phosphorylation of Akt, Clin. Cancer Res. 21 (2015) 4676–4685.

[6] Y. Goto, T. Ando, H. Izumi, X. Feng, N. Arang, M. Gilardi, Z. Wang, K. Ando, J. S. Gutkind, Muscarinic receptors promote castration-resistant growth of prostate cancer through a FAK–YAP signaling axis, Oncogene 39 (2020) 4014–4027.

[7] A. Paschos, R. Pandya, W.C.M. Duivenvoorden, J.H. Pinthus, Oxidative stress in prostate cancer: changing research concepts towards a novel paradigm for prevention and therapeutics, Prostate Cancer Prostatic Dis. 16 (2013) 217–225.

[8] L. Khandrika, B. Kumar, S. Koul, P. Maroni, H.K. Koul, Oxidative stress in prostate cancer, Cancer Lett. 282 (2009) 125–136.

[9] J.L. Meitzler, S. Antony, Y. Wu, A. Juhasz, H. Liu, G. Jiang, J. Lu, K. Roy, J. H. Doroshow, NADPH oxidases: A perspective on reactive oxygen species production in tumor biology, Antioxid. Redox Signal. 20 (2014) 2873–2889.

[10] A. Fontayne, P.M. Dang, M.A. Gougerot-Pocidalo, J. El-Benna, Phosphorylation of $p47^{phox}$ sites by PKC α, βII, δ, and ζ: Effect on binding to $p22^{phox}$ and on NADPH oxidase activation, Biochemistry 41 (2002) 7743–7750.

[11] J. Gautam, S. Banskota, P. Chaudhary, S. Dahal, D.-G. Kim, H.-E. Kang, I.-H. Lee, T.-G. Nam, B.-S. Jeong, J.-A. Kim, Antitumor activity of BJ-1207, a 6-amino-2,4,5-trimethylpyridin-3-ol derivative, in human lung cancer, Chem. Biol. Interact. 294 (2018) 1–8.

[12] H. Lee, S. Banskota, D.G. Kim, J.H. Been, Y.J. Jin, J. Gautam, H. Jang, T.-G. Nam, J.-A. Kim, B.-S. Jeong, Synthesis and antiangiogenic activity of 6-amido-2,4,5-trimethylpyridin-3-ols, Bioorg. Med. Chem. Lett. 24 (2014) 3131–3136.

[13] G.K. Mittapalli, D. Vellucci, J. Yang, M. Toussaint, S.P. Brothers, C. Wahlestedt, E. Roberts, Synthesis and SAR of selective small molecule neuropeptide Y Y2 receptor antagonist, Bioorg. Med. Chem. Lett. 22 (2012) 3916–3920.

[14] J.I. Perlmutter, L.T. Forbes, D.J. Krysan, K. Ebsworth-Mojica, J.M. Colquhoun, J. L. Wang, P.M. Dunman, D.P. Flaherty, Repurposing the antihistamine terfenadine for antimicrobial activity against Staphylococcus aureus, J. Med. Chem. 57 (2014) 8540–8562.

[15] G.W. Gribble, R.M. Leese, B.E. Evans, Reactions of sodium borohydride in acidic media; IV. Reduction of diarylmethanols and triarylmethanols in trifluoroacetic acid, Synthesis (1977) 172–176.

[16] J.Z. Long, L.X. Jin, A. Adibekian, W. Li, B.F. Cravatt, Characterization of tunable piperidine and piperazine carbamates as inhibitors of endocannabinoid hydrolases, J. Med. Chem. 53 (2010) 1830–1842.

[17] A. Orjales, R. Mosquera, A. Toledo, M.C. Pumar, N. Garcia, L. Cortizo, L. Labeaga, A. Innerarity, Synthesis and binding studies of new [(aryl)(aryloxy)methyl] piperidine derivatives and related compounds as potential antidepressant drugs with high affinity for serotonin (5-HT) and norepinephrine (NE) transporters, J. Med. Chem. 46 (2003) 5512–5532.

[18] S. Shah, C. Lee, H. Choi, J. Gautam, H. Jang, G.J. Kim, Y.-J. Lee, C.L. Chaudhary, S. W. Park, T.-G. Nam, J.-A. Kim, B.-S. Jeong, 5-Hydroxy-7-azaindolin-2-one, a novel hybrid of pyridinol and sunitinib: Design, synthesis and cytotoxicity against cancer cells, Org. Biomol. Chem. 14 (2016) 4829–4841.

[19] The DeepZema® (https://deepzema.io) is a web-based integrated platform by introducing artificial intelligence to a traditional computational drug discovery solution that can improve the accuracy of prediction throughout the entire process of new drug discovery and development from hit discovery, lead optimization, selectivity prediction, and ADME/Toxicity.

[20] J. Alvarsson, S.A. McShane, U. Norinder, O. Spjuth, Predicting with confidence: using conformal prediction in drug discovery, J. Pharm. Sci. 110 (2021) 42–49.

[21] O. Trott, A.J. Olson, AutoDock Vina: improving the speed and accuracy of docking with a new scoring function, efficient optimization and multithreading, J. Comput. Chem. 31 (2010) 455–461.

[22] Y. Goto, T. Ando, H. Izumi, X. Feng, N. Arang, M. Gilardi, Z. Wang, K. Ando, J.S. o. Gutkind, Muscarinic receptors promote castration-resistant growth of prostate cancer through a FAK–YAP signaling axis, Oncogene 39 (2020) 4014–4027.

[23] M.H. Zhu, I.K. Sung, H. Zheng, T.S. Sung, F.C. Britton, K. O'Driscoll, S.D. Koh, K. M. Sanders, Muscarinic activation of $Ca^{2+}$-activated $Cl^{-}$ current in interstitial cells of Cajal, J. Physiol. 589 (2011) 4565–4582.

[24] A. Petry, A. Görlach, Regulation of NADPH oxidases by G protein-coupled receptors, Antioxid. Redox. Signal. 30 (2019) 74–94.

[25] R. Serù, P. Mondola, S. Damiano, S. Svegliati, S. Agnese, E.V. Avvedimento, M. Santillo, HaRas activates the NADPH oxidase complex in human neuroblastoma cells via extracellular signal-regulated kinase 1/2 pathway, J. Neurochem. 91 (2004) 613–622.

[26] Procedures for the synthesis of 3A and 3J are provided here. Synthetic procedures for all compounds are described in Supplementary Material.